General Disclaimer

One or more of the Following Statements may affect this Document

- This document has been reproduced from the best copy furnished by the organizational source. It is being released in the interest of making available as much information as possible.

- This document may contain data, which exceeds the sheet parameters. It was furnished in this condition by the organizational source and is the best copy available.

- This document may contain tone-on-tone or color graphs, charts and/or pictures, which have been reproduced in black and white.

- This document is paginated as submitted by the original source.

- Portions of this document are not fully legible due to the historical nature of some of the material. However, it is the best reproduction available from the original submission.

PYROXENES AND OLIVINES IN CRYSTALLINE ROCKS FROM OCEAN OF STORMS

Neville L. Carter, Louis A. Fernandez, Hans G. Ave'Lallemant[1], and Irene S. Leung
Dept. of Geology and Geophysics, Yale University, New Haven, Conn.

ABSTRACT

Apollo 12 crystalline rocks 12044,4, 12063,18, 12057,31 and 12057,35 have been examined in detail to determine the petrology and deformational state principally of the pyroxenes and olivines. All four rocks have subophitic textures and are composed predominantly of intermixed pigeonite and augite, calcic plagioclase and 0% to 30% olivine; ilmenite, cristobalite and glass are accessories. Many pyroxenes are elongated parallel to c and contain (100) growth twins along which pigeonite has exsolved. The liquidus fractionation trend (commonly discontinuous) normal to (100) is subcalcic augite → Fe-rich pigeonite → Fe-rich subcalcic augite and calcic pigeonite → ferrohedenbergite. The elements Ti, Al, and Cr are enriched in augite relative to pigeonite and the distribution of Ti and Al suggests that the low pressure coupled substitution $2\,Al + Ti \rightleftharpoons 2\,Si + R^{+2}$ dominates.

There is no evidence for appreciable static deformation having affected the silicates in any of the specimens studied. Structures similar to those induced by plastic deformation are ascribed to rapid growth and quenching phenomena. Irregular chattermarks subparallel to {001} in augite surrounded by pigeonite are believed to originate by compressive strains parallel to c produced by differential thermal contractions of augite and pigeonite during cooling. The fabrics of olivines in 12044 and olivines and pyroxenes in 12063 are very weak indicating growth essentially in situ. Rock 12057,31 from the regolith has been shocked heavily as indicated by shock mosaicism, deformation twins and faults; there is no evidence of shock damage to the other specimens. The spread of whole rock K/Ar ages observed by others is not due to shock deformation as suggested but is attributed to selective diffusion of argon from interstitial glass with the greatest losses probably occurring from specimens residing on the lunar surface.

1. Dept. of Geology, Rice University, Houston, Texas.

INTRODUCTION

In this paper we shall discuss the results of detailed optical, X-ray and electron microprobe studies of four crystalline rocks (12063,18, 12044,4, 12057,35, and 12057,31) from the Ocean of Storms. The primary purpose of our work is to evaluate the extent to which static and dynamic deformational processes have operated on lunar rocks since their time of crystallization but an essential first step involves petrological examinations of the specimens. From the point of view of the tectonic history and thermal evolution of the moon, the presence or absence of microstructures and fabrics induced by static deformational processes are most important. Experiments in the last decade (for a recent review, see Carter, 1971) on quartz, olivine, orthopyroxene, clinopyroxene, and plagioclase have shown that the plastic deformation mechanisms generally vary with temperature and strain rate and, in some cases, with pressure. In addition, the diffusion-controlled recovery process, polygonization, has been produced in some of those materials and syntectonic recrystallization of aggregates of quartz, olivine, and enstatite has given rise to strong preferred crystal orientations. These experimentally produced fabrics as well as polygonization and many of the plastic flow mechanisms have also been observed in tectonites allowing inferences to be drawn concerning the physical conditions during natural deformations and the tectonic history of the materials. However few, if any, of these features were observed in crystalline rocks from the Sea of Tranquillity (Carter et al., 1970), a negative observation of considerable importance for interpretations of the origin of the moon. As we shall show here, this conclusion appears to hold as well for the crystalline rocks (examined by us) from the Ocean of Storms.

PETROLOGY OF THE SPECIMENS

All of the rocks examined by us are medium-grained basalts with subophitic texture and are composed dominantly of intermixed pigeonite and augite and calcic plagioclase. Mg-rich olivines, euhedral to subhedral in shape, range in abundance from about 30% in 12057,35 through 5% to 10% in 12044,4 and 12063,18 to 0% in 12057,31 and Fe-rich olivine occurs with glass in the interstices of all specimens except 12057,31. Ilmenite, cristobalite and blebs of troilite with native iron inclusions are common accessories, the last two of these being interstitial.

Olivine and glass

Two distinct generations of olivines are observed in three of the specimens; an early crystallizing euhedral to subhedral forsteritic olivine and a late-stage fayalite (typical analyses are shown in Table 1). The forsteritic olivines are

strongly zoned in both major and minor elements. Individual crystals have cores of Fo_{67} ranging to Fo_{58} at the rims; this range also reflects the entire composition range measured. The fayalitic olivines ($Fo_{0.5}$ to $Fo_{2.0}$), commonly associated with cristobalite, Fe-rich pyroxenes, glass, and a high barium-potassium phase (alkali feldspar?; Hollister et al., 1971), are a product of the crystallization of late stage interstitial residual liquids. This last liquid probably crystallized the fayalite leaving a liquid which is now a siliceous, K-rich glass with occasional feldspar crystals. The hiatus in the crystallization trend between intermediate forsterite and late fayalite is also commonly observed in terrestrial tholeiite suites (Kuno, 1969).

The minor element contents of the olivines are similar to those found for Apollo 11 rocks (Haggerty et al., 1970; Keil et al., 1970). They are enriched in Cr but depleted in Ca and Ni relative to terrestrial olivines. The lower Ni content is attributed to low total Ni in the lunar rocks. The low Ca may be due to co-precipitation of calcic plagioclase and/or calcic pyroxene. The very high Cr content is attributed by Haggerty et al., (1970) to its being in a divalent rather than trivalent state.

Typical analyses of the silicate glass within the fayalite are given in Table 2 although these are not of the best quality because of the small (<0.02mm) size of the blebs. Several point count analyses on 12044,4 indicate that fayalite and glass account for ≈3% of the total rock volume with the glass making up about 0.5 wt% of the rock. Based on this estimate, averages given by Roedder and Weiblen (1970), and the average K_2O content of lunar basalts and plagioclases, it appears that more than 50% of the K_2O in these rocks may be contained in the glass. This conclusion may have an important bearing on whole rock potassium-argon ages as will be discussed subsequently.

Clinopyroxene

Clinopyroxene, the dominant phase in the rocks studied, varies in shape from large (up to 1 cm) inequant anhedral plates elongated parallel to c through subhedral prismatic crystals of intermediate size to small interstitial equant grains. These pyroxenes commonly contain (100) growth twins with a very thin (ca. 10μ) plate of pigeonite occupying the position of the composition plane (Fig.1A). Near the end of one crystal, the thin pigeonite nucleus becomes thicker giving the core a funnel-shaped configuration similar to the "martini glass" clinopyroxene described by Bence and Papike (1971). Lamellar structures subparallel to {001} commonly occur in the augite on either side of the composition plane (NW-trending

structures in Fig. 1A). These features are distinct from exsolution lamellae parallel to {001} (Fig. 1C) found in some of the augite crystals.

The clinopyroxenes consist either of composite crystals whose compositions plot near the center of the pyroxene quadrilateral (Fig. 2) or as epitaxially related primary phases composed predominantly of pigeonite and augite (Tables 3 and 4). The composite crystals are the result of subsolidus exsolution of Ca-rich and Ca-poor phases. This has been verified by electron microscopy (cf. Radcliffe et al., 1970; Ross et al., 1970; Fernandez-Moran, 1970) and X-ray precession (cf. Ross et al., 1970; Carter et al., 1970) studies of Apollo 11 pyroxenes and similar studies of Apollo 12 pyroxenes (these proceedings). The presence of pigeonite or augite as primary phases is apparently restricted to the high-temperature, early-crystallizing Mg-rich clinopyroxenes in these samples. The degree to which these phases approach the single phase compositions probably depends on the temperature of crystallization and rates of crystal growth and cooling.

The results of some 250 microprobe analyses on eight different crystals of 12063,18 and 12044,4 are presented in Figure 2 (top). A liquidus fractionation trend as reflected in these quenched composite crystals is: subcalcic augite → Fe-rich pigeonite → Fe-rich subcalcic augite and Fe-rich calcic pigeonite → ferrohedenbergite. Because of the extreme zoning in many of the crystals, some show nearly the complete fractionation trend. For example, a microprobe traverse from core to rim (nearly normal to (100) of the crystal shown in Figure 1A is plotted on the pyroxene quadrilateral (dashed lines and open circles) in Figure 2 (bottom). The very thin nucleus of pigeonite is sheathed by a subcalcic augite (with some exsolved pigeonite) which, in turn, is surrounded by a zone of calcic pigeonite that grades into an augite-pigeonite mixture and ends in ferrohedenbergite. The variations in concentration of the major elements of this crystal, probed nearly normal to the twin plane from rim to rim are shown in Figure 3. From core to rim, the trend is calcic pigeonite ($Ca_{20}Mg_{50}Fe_{30}$) → sub-calcic augite ($Ca_{25}Mg_{47}Fe_{28}$) → Fe-rich pigeonite ($Ca_{10}Mg_{48}Fe_{42}$) → Fe-rich subcalcic augite ($Ca_{22-24}Mg_{15-40}Fe_{40-60}$) → ferrohedenbergite ($Ca_{37}Mg_6Fe_{57}$).

The very thin pigeonite nuclei common to elongated clinopyroxene crystals with (100) growth twins are believed to be due to high temperature exsolution. As pointed out by M. Ross (personal communication), twin composition planes are regions of relatively high structural distortion and might provide excellent sites for exsolution. The depletion of Fe and Mg and enrichment of Ca, Ti and Al in the augite immediately adjacent to the nucleus (Fig. 2B, 3) supports this hypothesis (see also Bence and Papike, 1971, Fig. 2). In addition, the pigeonite nucleus is

discontinuous in some of our crystals. For crystals with "martini glass" configurations, the funnel-shaped portions may be primary, having nucleated on the exsolved stem of pigeonite. This topic, with its associated conjectures, will be discussed more fully by Fernandez and Carter (in preparation).

A somewhat limited but different fractionation trend is revealed by a crystal composed of nearly equal amounts of primary pigeonite and augite (Fig. 1B). The exceptionally thick pigeonite nucleus (0.25mm), although sheathed on its prism faces by augite, has continued to grow parallel to c. Because of the thickness of the nucleus, fractionation trends could be determined both normal and parallel to c and these are given in Figure 4. The trend normal to c and (010) of augite from core to rim (Fig. 4, center of A-D to A or D) is from pigeonite to high-Ca pigeonite to subcalcic augite. Parallel to c, from center to edge (Fig. 4, E-F), pigeonite changes from low-Ca pigeonite to high Ca pigeonite (≈20 mol% Ca) and then reverses to low-Ca pigeonite becoming progressively Fe-rich as the Ca content increases slightly. This trend is also shown by the dotted line and solid circles in Figure 2 (lower). These trends suggest the following sequence during crystallization: (1) pigeonite crystallized first, initially becoming more calcic both normal and parallel to c; (2) augite became stable and nucleated epitaxially on the pigeonite prism faces while the pigeonite continued to grow parallel to c; (3) the augite became more calcic with continued crystallization while the pigeonite reversed, becoming less calcic; and (4) at the rims, the augite became sub-calcic and the pigeonite, calcic, both phases becoming Fe-rich.

Step (4) above, in which both augite and pigeonite trend toward the center of the quadrilateral, as observed for many of the pyroxene crystals (Fig. 2, top), is most likely the result of rapid crystallization. Steps (1) through (3) are, however, believed to represent relatively slow, stable crystallization. The persistence of pigeonite to grow in the c-direction and its reversal in calcium content (also observed for our "martini glass"-like crystal) contrasts with the trend observed by Bence and Papike, (1971), in which the pigeonite nucleus of the "martini glass" clinopyroxene became increasingly Ca-rich, presumably growing metastably in the augite stability field. For our crystal, the reversal in Ca content has probably resulted from the onset of crystallization of calcic clinopyroxene and/or calcic plagioclase.

Although it appears as if the Ca-rich augite and Ca-poor pigeonite may represent an earlier, more stable stage of crystallization relative to most of the crystals, there is no indication that this stage took place at depth. To be sure, the augite compositions are high in Cr_2O_3 and Al_2O_3 (Table 4) relative to

other augites of equivalent Mg/Fe ratios (Table 3). However, most of the Al appears to be in tetrahedral coordination and both Al and Ti increase toward the rims suggesting that the controlling parameters were silica activity and growth rate rather than pressure. The distributions of Cr, Al, Ti and Mn in the calcic pyroxenes suggest the low pressure coupled substitution

$$2Al + Ti \rightleftharpoons 2Si^{+4} + R^{+2},$$

as was observed for Apollo 11 pyroxenes.

In addition to the chemical zoning, the pyroxenes are generally very strongly zoned optically with V_γ ranging widely. The highest values of V_γ or $2V_\gamma$ in the augites are most commonly found near the centers of the grains (Figs. 5A,C,F) decreasing outward (perhaps corresponding to a decrease in Ca). However, this trend may reverse or oscillate, especially for crystals cut nearly normal to c, as observed previously for Tranquillity pyroxenes (Carter et al., 1970, Fig. 4C). The pyroxenes also commonly show disorientations of the optical and crystallographic axes (Fig. 1D). As for Apollo 11 pyroxenes, these disorientations can generally be described as a rotation about the β = b axis (Fig. 5D) forming extinction bands subparallel to {001}. However, as also observed previously, the rotations occasionally appear to be irregular as illustrated by measurements of the principal indicatrix axes (Fig. 5G) in the various zones of the crystal sketched in Fig. 5E.

DEFORMATION OF THE SPECIMENS

Static Deformation

The bending of the pyroxene crystal structure about b described above, if due to static plastic deformation, is consistent with translation-gliding on the{100} plane in the [001] direction; this slip system is observed in tectonites and in experiments at high temperatures and low strain rates (Raleigh and Talbot, 1967). However, such an interpretation can be excluded for reasons similar to those advanced for Apollo 11 pyroxenes (Carter et al., 1970). First, optical and X-ray precession and Laue studies of the olivine grains in our Apollo 12 samples indicate that, with few exceptions, the olivines are totally undeformed. One grain of 100 in specimen 12063,18 and three grains of 200 in 12057,35 contained kinks parallel to (100) and the slip system determined is {0kl}[100], the high temperature-low strain rate system in olivine (Raleigh, 1968; Carter and Ave'Lallemant, 1970). Olivine deforms much more readily under both static and dynamic conditions than pyroxenes but only very slight deformation of olivine has occurred, probably during quenching of these rocks.

The second line of evidence comes from the lack of thin polysynthetic deformation twins according to the system {100}[001]in Apollo 12 pyroxenes. This mechanism is a common mode of flow of clinopyroxenes at high temperatures and low strain rates (Raleigh and Talbot, 1967) but only {100}[001] growth twins were observed (e.g., Figs. 1A,6A). Finally, thin laths of plagioclase and skeletal ilmenite crystals in highly disoriented regions of the pyroxene crystals are undistorted whereas they should be bent or broken in a systematic fashion if the pyroxene disorientations are due to plastic deformation. For example, the ilmenite crystal shown in Figure 6A (NE-trending crystal near top) is undisturbed although embedded in a clinopyroxene crystal twinned through 8° (flat stage extinction difference) and further distorted through a total rotation of 34°. By analogy with similar pyroxene disorientations in chondrules and in quenched natural and artificially produced melts (Carter et al., 1970), the disorientations in Apollo 12 pyroxenes are ascribed to rapid growth and quenching phenomena.

As mentioned previously, in addition to {001} exsolution lamellae in the augite of the complexly zoned and twinned crystals, other structures resembling 'chattermarks' are developed subparallel to {001} (Fig. 6B). These features (the small EW-trending steps in Figure 6B) are irregular with disorientations up to 6° and having rather sharp boundaries, occasionally fractures, on one side and grading into the host orientation on the other. The sharper boundaries bend abruptly into the pigeonite nucleus at the composition plane and more gradually into the

pigeonite-augite intermixed pyroxene on the other side. Some of the 'chattermarks' penetrate the enclosing intermixed phase but, in general, a sharp coherent boundary separates the two with the mixed phase being relatively undeformed, thus ruling out a conventional static deformational origin of the 'chattermarks'. Electron microprobe traverses across these features show no changes in chemical composition. X-ray precession photographs were taken of the h0l net of one of these 'chattermarked' crystals having only a small border of the mixed phase. In Figure 7A, the entire crystal was irradiated and in Figure 7B the crystal was moved so as to irradiate dominantly one augite subindividual and the bordering mixed phase. Distortion and streaking of the spots is greater in Figure 7A probably reflecting rotations in the 'chattermarked' region.

We believe that the 'chattermarks' have originated by differential thermal contraction of the augite, pigeonite and intermixed phases during cooling; there appears to be no other satisfactory explanation for their origin unless they are rapid growth phenomena. The structures probably formed by compression parallel to c at fairly high temperatures during cooling of the basalts as lower temperatures would have resulted in fracturing of these brittle silicates. Unfortunately, the lattice constants of pigeonite and augite are not known accurately at temperatures above 670°C. However, Prewitt et al., (1970) give the cell dimensions of pigeonite ($Ca_{3.5}Mg_{18}Fe_{78.5}$) and augite ($Ca_{48}Mg_{16.5}Fe_{35.5}$) at 670°C and 25°C. In this temperature range, there is no difference in contraction in the b direction, c (pig) contracts 0.08Å compared to 0.02Å (aug.), and a (pig.) contracts by 0.10Å compared to 0.06Å (aug.); the a axes are the same length at 670°C where pigeonite inverts from $P2_1/c$ to C2/c (Prewitt et al.,1970). The greatest differential thermal contraction (0.06Å) is, therefore, parallel to c with the pigeonite contracting more than the augite and thereby exerting a compressive strain on it. The differential contraction parallel to c is about 10^{-4} Å/°C corresponding to a strain of about 2×10^{-5}/°C. Assuming that these differences in contraction rate persist to homogenization (ca. 1200°C; Ross et al., 1971) and that the structures developed at about 700°C, the total strain accumulated during the 500°C temperature drop would be 10^{-2}. The stress parallel to c resulting from this strain (calculated using the stiffness coefficient, C_{33}, for aegerite; Birch, 1966) amounts to a compressive stress of about 11 kb on the augite side and an equal tensile stress on the pigeonite side. This crude estimate is likely to be a maximum for the following reasons: (1) the strain calculated is based on cell constants of rather pure augite-pigeonite "end-members" whereas the pyroxenes under consideration are of mixed types; (2) the strain was calculated using cell constants in the temperature interval 25°C - 670°C - the differences in expansion probably decrease

at higher temperatures to homogenization; and (3) some of the strain may be relieved by reorientation of composition planes of exsolution lamellae (M. Ross, personal communication) or possibly by development of anti-phase domains in the pigeonite (Christie et al., 1971). Thus, the situation is complex but it appears as if the type of strain induced by differential thermal contraction is of the correct sign to have produced the 'chattermarks' irrespective of the tenuous nature of the stress estimate.

Fabrics

In Figure 8 we present the fabrics of olivine grains in specimen 12057,35 (A) and olivines and pyroxenes in 12063,18 (B-D). The olivine fabrics for both specimens are very weak and, although there appears to be some preferred orientation, it is much weaker than is observed for most cumulate fabrics. These results are in contradiction to those reported by Butler (1970) in which he indicates that the olivine a-axes in each of three aggregates (specimen numbers not given) are subparallel. The olivines in our specimens have not been recrystallized and so the weak orientations observed are attributed to very slight gravitational settling on the generally well-developed crystal faces (010), (021) and (110).

The olivine crystals are generally equant but the pyroxene grains, which also have not recrystallized, are commonly highly inequant being elongate parallel to c. If there were significant gravitational settling or flow during and after crystallization of the pyroxenes a strong c-axis girdle or maximum should be developed as well as strong preferred orientations of (100) planes and β-axes. Inspection of Figure 8C-D reveals that this is not the case; the fabrics are nearly random as were those for rock 10047 (Carter et al., 1970). The nearly random orientation of these elements, the weak orientations of the olivines and the subophitic texture indicates that these crystals did not settle appreciably or flow in a magma but grew essentially in situ. These results contrast with those of Greenwood et al., (1971) who measured the long axes of olivine and pyroxene phenocrysts in porphyritic basalt 12052 and found a foliation which they interpret to be due to flow. The foliation is, however, very weak and a fabric analysis is required to confirm differences in the crystallization history of the subophitic and porphyritic basalts.

namic deformation

Of the rocks under discussion, only 12057,31 shows evidence of strong shock, the remaining specimens being only very lightly fractured, if at all. The "Heidelberg Group" (1971) has reported microcraters on the surface of 12063 and Taylor et al. (1971; personal comm.) have observed localized twinning in ilmenite (probably near the rock surface), whereas Hollister et al., (1971) and the writers have found no evidence for shock deformation in 12063. This discrepancy clearly points up the need for caution concerning generalizations drawn from studies of single sections and for a knowledge of the distance of any section from the rock surface. Most of the grains in 12057,31 are fractured, some contain deformation twins (Fig. 6C) and some of the pyroxenes show the mosaic texture associated with

strong shock deformation (Fig. 6C; Carter et al., 1968). Many of the clinopyroxene grains contain thin polysynthetic twins parallel to {001} and a few parallel to {100}, the twins commonly pinching out before reaching the grain boundaries. In some grains, the twins are associated with and are highly developed near shear fractures and the sense of shear for twinning is consistent with that producing the fractures (Fig. 9A). Compression and tension axes deduced from the twins (Raleigh and Talbot, 1967) in 25 grains are also in agreement with the orientation of σ_1 (arrows) inferred from the shear fractures, indicating that the twins are indeed deformation twins.

The calcic plagioclase crystals do not contain kink bands or planar features but some of the small pericline twins could be due to shock. Most of the plagioclases are strongly fractured (Fig. 6D) and most of the shear fractures have non-rational orientations. Figure 9B shows the orientations of twenty-six shear fractures in plagioclase crystals and two in pyroxenes, the sense of shear being indicated by the arrows. The analysis leads to the statistical orientation of the shear fractures shown and once again, the orientation of σ_1 should be approximately E-W. Thus, the deformational features in this specimen are consistent with its having been deformed by a strong shock wave propagating in an E-W direction (the actual direction of shock on the lunar surface is not known).

K-Ar Ages

Recent results from K/Ar dating of Apollo 11 rocks (e.g. Turner, 1970; Schaeffer et al., 1970) and Apollo 12 rocks (Schaeffer et al., 1970) have shown that large (up to 48%) amounts of radiogenic argon has been lost from some of the samples. The whole rock ages determined vary widely and the mean ages from the Ocean of Storms (variations from 1.4 - 3.0 b.y.) are about one billion years younger than those from the Sea of Tranquillity (variations from 2.2 to 4.0 b.y.; Schaeffer et al., 1970). Turner (1970) suggested that the argon loss in some of the Apollo 11 samples may have been due to shock deformation and Schaeffer et al. (1970), following Turner, suggested that the Apollo 12 rocks may have been shocked more severely.

It has been shown previously from studies on chondritic meteorites (Carter et al., 1968) that the gas-retention ages correlate well with the degree of shock deformation as estimated from petrographic criteria based on studies of experimentally shocked material. That is, those specimens having suffered no shock to light shock deformation had very old ages whereas those heavily shocked had young ages. Unfortunately, there seems to be no such correlation between the K/Ar ages determined by others and shock effects on Apollo 11 and Apollo 12 crystalline rocks studied by us. Rocks 10047 and 10017 have very young apparent ages (Schaeffer et al., 1970; Turner, 1970) but show no evidence

of shock deformation whatever (Carter et al., 1970). Similarly, we found no evidence of shock in crystalline rocks 10067 and 10020 which have intermediate and long gas-retention ages (Schaeffer et al., 1970). As indicated above, rocks 12044,4 and 12063,18 show no evidence of shock yet these rocks have yielded intermediate whole rock K/Ar ages (Schaeffer et al., 1970). More recently, Fernandez et al. (1971) have studied thin sections of Apollo 11 and 12 crystalline rocks for which K-Ar dates are available and found evidence for zero to only light shock deformation (some fracturing) in all of the specimens. According to the results of Carter et al. (1968) this degree of shock deformation should have resulted in virtually no gas loss. Part of the discrepancy could be due to analysis of different portions of the same lunar rock but, in general, we suggest that shock deformation is not primarily responsible for the variation in gas loss of the lunar specimens.

What then is the mechanism responsible for the variable gas loss? We are not certain but we feel that it may be due to selective diffusion of argon from the relatively potassium-rich glass as has been suggested previously by Roedder and Weiblen (1970). As shown by Albee et al. (1970) and Eberhardt et al. (1970) the K/Ar ages determined from the plagioclases of Apollo 11 are distinctly older than are the whole rock ages. For rock 10017 (which according to Carter et al., 1970, shows no shock effects), for example, the whole rock age was 2.3 - 2.4 b.y. (Turner, 1970; Albee et al., 1970) whereas the plagioclase age was 3.2 b.y. (Albee et al., 1970) and Turner's (1970) corrected age was 3.23 b.y. Rock 10017 contains 2407 ppm K and the plagioclase, which makes up 23% of the rock contains 1920 ppm K or accounts for a total of 444 ppm leaving 1963 ppm or about 80% of the potassium in other phases, most of which presumably resides in the glass. On the other hand, rock 10044 had a whole rock age of 3.45 - 3.62 b.y., a pyroxene K/Ar age of 3.6 b.y. (Albee et al., 1970) and a corrected age of 3.74 b.y. (Turner, 1970). This rock contains 913 ppm K about 80% of which is contained in the 33% plagioclase which contains 2160 ppm K. There are few other data for which a comparison of whole rock ages with those obtained from mineral separates can be made (for a more detailed discussion see Fernandez et al., 1971) but it appears as if the concentration of K_2O in glass is the most probable explanation for the losses. If this conclusion is correct, it would be expected, from our studies on Apollo 12 material, that the whole rock apparent ages should be younger than those from Apollo 11 material because of the higher percentage of glass in the specimens.

Little is known about the diffusion coefficients of argon in glasses but it appears as if they are appreciably higher than in plagioclases. For Moldavite, the analyzed glass nearest in composition to the lunar glasses, the activation energy (E*) for argon diffusion is 30 Kcal/mole and the diffusion coefficient

(D) at 20°C is 8 x 10^{-27}/cm^2/sec. (Fechtig and Kalbitzer, 1966). For anorthite, E* is 56 Kcal/mole and $D_{20°C}$ is <10^{-30} cm^2/sec. The structure of glasses, whether the random network structure of Zachariasen (1932) or the discrete ion arrangement of Bockris et al., (1955), should be more conducive to argon loss than the ordered structure of plagioclase. In either model, the glass structure can be regarded as very small domains of short range order whose boundaries, like subgrain boundaries, serve as avenues for relatively rapid diffusion. This, coupled with the small size of the lunar glass blebs compared with the plagioclases should allow relatively easy escape of the argon. The spread in ages of the various rocks could then be accounted for by the proportion of glass present and/or the distance of the rock from the lunar surface. Glass in rocks resting on the lunar surface should lose appreciably more argon in long periods of time than should those shielded from the very hot (ca. 400°K) lunar day temperatures. This hypothesis, if correct, might provide a quantitative means for estimating long residence times on the lunar surface of unshocked, glass-bearing rocks.

CONCLUSIONS

We conclude that all of the petrological, chemical and structural features observed in the Apollo 12 crystalline rocks examined by us are attributable to rapid growth and quenching phenomena. In accord with the interpretation based on studies of rocks from Mare Tranquillitatis (Carter et al., 1970) there is no evidence that appreciable static deformational processes have operated on the crystalline rocks of the Ocean of Storms. From this we infer that the rocks from both sites have not been involved in any substantial tectonic activity since their rapid crystallization some three to four billion years ago.

ACKNOWLEDGEMENTS

We are indebted to Drs. A.E. Bence and M. Ross for very helpful discussions and constructive criticism of the manuscript. This research was supported by NASA Contract NAS 9-9937.

REFERENCES

Albee, A.L., Burnett, D.S., Chodos, A.A., Eugster, L.G., Huneke, J.C., Papanastassiou, D.A., Podosek, F.A., Price Russ II., G., Sanz, H.G., Tera, F., Wasserburg, G.J., (1970), Ages irradiation history, and chemical composition of lunar rocks from the Sea of Tranquillity, Science, 167, 463-66.

Bence, A.E. and Papike, J.J. (1971), A martini glass clinopyroxene from the moon. Earth Planet. Sci. Lett., 10, 245-251.

Birch, Francis (1966), Compressibility, elastic constants, Mem. Geol. Soc. Amer., 97, 97-173.

Bockeris, J.M., MacKenzie, J.D. and Kitchener, J.A. (1955), Viscous flow in silica and binary liquid silicates, Trans. Faraday, Soc., 51, 1734-1748.

Butler, P., Jr. (1970), Fabric and compositions of olivines in three Apollo 12 igneous rocks (Abs.), Geol. Soc. Amer. Annual Meeting, 1970.

Carter, N.L. (1971), Static deformation of silica and silicates, in press, Jour. Geophys. Res.

Carter, N.L., Raleigh, C.B., and DeCarli, P.S. (1968), Deformation of olivine in stony meteorites, Jour. Geophys. Res., 73, 5439-5461.

Carter, N.L. and Ave'Lallemant, H.G. (1970), High temperature flow of dunite and peridotite, Bull. Geol. Soc. Amer., 81, 2181-2202.

Carter, N.L., Leung, I.S., Ave'Lallemant, H.G., and Fernandez, L.A. (1970), Growth and deformational structures in silicates from Mare Tranquillitatis, Proc. Apollo 11 Lunar Sci. Conf., Geochim. Cosmochim. Acta Suppl. I, Vol. 1, Pergamon, 267-285.

Christie, J.M., Fisher, R.M., Griggs, D.T., Heuer, A.H., Lally, J.S., and Radcliffe, S.V. (1971), Comparative electron petrography of Apollo 11, Apollo 12 and Terrestrial Rocks, Second Lunar Sci. Conf. (unpublished proceedings).

Eberhardt, P., Geiss, J., Graf, H., Grogler, N., Krahenbuhl, U., Schwaller, H., Schwarzmuller, J., and Stettler, A. (1970), Trapped solar wind noble gases exposure age and K/Ar age in Apollo 11 Lunar fine material, Proc. Apollo 11 Lunar Sci. Conf., Geochim. Cosmochim. Acta Suppl. 1, Vol. 1, 1033-1070, Pergamon.

Fechtig, H., and Kalbitzer, S. (1966), The diffusion of argon in potassium-bearing solids: in Potassium Argon Dating, O.A. Schaeffer and J. Zahringer, Eds., Springer Verlag. Press., 68-107.

Fernandez, L.A., Ave'Lallemant, H.G., and Carter, N.L. (1971), Origin of K/Ar gas retnetion ages of Apollo 11 and 12 rocks, in press.

Fernandes-Moran, M., Ohtsuki, S., Hafner, S., and Virgo, D. (1970), High-voltage electron microscopy and electron diffraction of lunar pyroxenes, Proc. Apollo 11 Lunar Sci. Conf., Geochim. Cosmochim. Acta, Suppl. 1, Vol. 1, 408-418, Pergamon.

Greenwood, W.R., Morrison, D.A., and Clark, A.L. (1971), Flow foliation in lunar surface rock from the Ocean of Storms, Apollo 12 Flight, Second Lunar Science Conference (unpublished proceedings).

Haggerty, S.E., Boyd, F.R., Bell, P.M., Finger, L.W., and Bryan, W.B., (1970), Opaque minerals and olivine in lavas and breccias from Mare Tranquillitatis, Proc. Apollo 11 Lunar Sci. Conf., Geochim. Cosmochim. Acta Suppl. 1, Vol. 1, 513-538, Pergamon.

Heidelberg Lunar Sample Investigation Group (1971), Meteorite impact craters, crater simulations and the meteoric flux in the early solar system, Second Lunar Science Conference (unpublished proceedings).

Hollister, L., Trzcienski, W., and Hargraves, R. (1971), Crystallization histories of samples 12063 and 12065, Second Lunar Science Conference (unpublished proceedings).

Keil, K., Bunch, T.E., and Prinz, M. (1970), Mineralogy and composition of Apollo 11 lunar samples, Proc. Apollo 11 Lunar Sci. Conf., Geochim Cosmochim Acta Suppl. 1, Vol. 1, 561-598, Pergamon.

Kuno, H. (1969), Differentiation of basalt magmas, in Basalts, The Poldervaart Treastise on Rocks of Basaltic Composition, H.H. Hess and A. Poldervaart, Eds., J. Wiley and Sons, 623-688.

Prewitt, C.T., Papike, J.J., and Ross, M. (1970), Cummingtonite: A reversible, nonquenchable transition from $P2_1/m$ to C2/m symmetry, Earth Planet. Sci. Lett., 8, 448-450.

Radcliffe, S.V., Heuer, A.H., Fisher, R.M., Christie, J.M., and Griggs, D.T., (1970), High voltage (800 kv) electron petrography of type B rock from Apollo 11, Proc. Apollo 11 Lunar Sci. Conf., Geochim. Cosmochim. Acta Suppl. 1, Vol. 1, 731-748, Pergamon.

Raleigh, C.B., (1968), Mechanisms of plastic deformation of olivine, Jour. Geophys. Res., 73, 5391-5406.

Raleigh, C.B. and Talbot, J.L. (1967), Mechanical twinning in naturally and experimentally deformed diopside, Amer. Jour. Sci., 265, 151-165.

Roedder, E. and Weiblen, P.W. (1970), Lunar petrology of silicate melt inclusions, Apollo 11 rocks, Proc. Apollo 11 Lunar Sci. Conf., Geochim. Cosmochim. Acta., Suppl. 1, Vol. 1, 801-838, Pergamon.

Ross, M., Bence, A.E., Dwornik, E.J., Clark, J.R., and Papike, J.J. (1970), Mineralogy of the lunar clinopyroxenes, augite and pigeonite, Proc. Apollo 11 Lunar Sci. Conf., Geochim. Cosmochim. Acta, Suppl. 1, Vol. 1, 839-848, Pergamon.

Ross, M., Huebner, J.S., and Dowfy, E. (1971), Melting and sub-solidus phase relations of augite and pigeonite from lunar rock 12021, Second Lunar Science Conference (unpublished proceedings).

Schaeffer, O.A., Funkhouser, J.G., Bogard, D.D. and Zahringer, J. (1970), Potassium-argon ages of lunar rocks from Mare Tranquillitatis and Oceanus Procellarum, Science, 170, 161-162.

Taylor, L.A., Kullerud, G., and Bryan, W.B. (1971), Mineralogy of two Apollo 12 samples, Second Lunar Science Conference (unpublished proceedings).

Turner, G. (1970), Argon 40/argon 39 dating of lunar rocks, Proc. Apollo 11 Lunar Sci. Conf., Geochim. Cosmochim. Acta Suppl. 1, Vol. 1, 1665-1684, Pergamon.

Zachariasen, W.H. (1932), The atomic arrangement in glass, Jour. Amer. Chem. Soc., 54, 3841-3851.

CAPTIONS FOR FIGURES

1. Photomicrographs of clinopyroxene crystals. Scale lines beneath photos represent 0.1 millimeter.
   A. NE-trending (100) twin in clinopyroxene crystal in 12044,4 with pigeonite nucleus along the composition plane. Nucleus is sheathed by augite with NW-trending 'chattermarks' which, in turn, is surrounded by an augite-pigeonite mixture (see Fig. 2).
   B. Thick pigeonite nucleus (gray) surrounded by augite (light) (see Fig. 2) in 12044,4.
   C. Exsolution lamellae (light NW-trending linear features in center) of pigeonite along {001} of augite host.
   D. Uniform undulatory extinction in EW zones; rotated about b by 23°, in pyroxene crystal from 12057,35.

2. Electron microprobe analyses of clinopyroxenes in specimens 12044,4 and 12063,18.
   Top: Compositional plots of more than 250 clinopyroxene analyses on pyroxene quadrilateral. Each point represents a 3-5μ area.
   Bottom: Open circles - dashed line - microprobe traverses from core to rim of pyroxene in Figure 1A. The trend subcalcic augite to ferrohedenbergite corresponds to traverse C to E or C to A in Figure 3. Filled circles - dotted line - traverse from core to rim in c direction of pyroxene in Figure 1B. The trend pigeonite to Fe-rich pigeonite corresponds to traverse E to F in Figure 4.

3. Variations in major and minor elements in a rim to rim traverse normal to twinned pyroxene crystal shown in Figure 1A. Point C marks the thin pigeonite nucleus (10-20μ) and B and D mark sharp chemical and optical discontinuities parallel to {100} which separate subcalcic augite with 'chattermarks' from pigeonite-augite. Each point represents an integrated analysis of 3 area and vertical scale is counts/20 sec. Analyses 1-9 in Table 3 represents the rim-core portion of the traverse. Analyses 1, 4 and 9 correspond to points A, B and C, respectively.

4. Variations in major and minor elements of thick pigeonite-cored clinopyroxene shown in Fig. 1B. Traverse A to D is from rim to rim, approximately normal to c, and (010) and traverse F to E is from core to rim parallel to c. Points B and C mark chemical and optical discontinuities at boundary between pigeonite core and subcalcic augite rim. Analyses from these two traverses are presented in Table 4. Analyses 1, 3, 5, 7, 8, 13 correspond to points A, B, C, D, E, F, respectively.

5. Optical zoning and disorientations in the ~~clinopyroxene~~ augite crystals in 12063,18.
   A. Zones of homogeneous extinction (solid lines) and of uniform optic axis angle (dotted lines).
   B,C,D. Areas of measurements (numbers in B) shown in D and optic axial angles (C). Rotations of optical and crystallographic elements in D are about b which is typical of most disoriented crystals.
   E,F,G. Areas of measurements (numbers in E) shown in G and optic axial angles (F). Rotations of principal optic directions in G are irrational as found in a few of the crystals.

6. Photomicrographs of structures in clinopyroxenes and shocked silicates. Scale lines beneath photos represent 0.1 millimeter.
   A. Thin ilmenite crystal (dark, NE-trending crystal near top) embedded in twinned and distorted (through 34°) clinopyroxene in 12063,18.
   B. 'Chattermarks' (EW-trending step-like features in same crystal as Fig. 1A. Note the sharp boundary (// E1003) between the 'chattermarked' augite and the relatively undistorted pigeonite-augite and the sharp bends of the 'chattermarks' near the pigeonite nucleus.
   C. Shocked pyroxene in 12057,31. The clinopyroxene crystal near the lower right contains polysynthetic twins on {001} whereas the large mottled crystal on the left is pyroxene with shock mosaicism.
   D. Distorted plagioclase crystal in 12057,31 with well-developed conjugate faults.

7. X-ray precession photographs of the h0l net of a pyroxene crystal from 12044,4. Zr-filtered Mo radiation (45 Kv/20 mA).
   A. Augite crystal containing 'chattermarks' twinned on (100) and containing about 5% exsolved pigeonite (4-day exposure).
   B. Rim of same crystal containing twin but also some of the pigeonite-augite sheathe. Pigeonite is about 10% and streaking is less intense (12-day exposure).

8. Fabrics of olivines (A,B) and pyroxenes (C,D) from rocks 12057,35 (A) and 12063,18 (B-D). Contours in B,C,D (including dashed lines) are at intervals of one percent per one percent area. Contours in A are at multiples of uniform distribution. Lower hemisphere equal area projections.
   A. Principal indicatrix axes in 200 grains in olivine of 12057,35.
   B. Principal indicatrix axes in 100 olivine grains from 12063,18.
   C. Principal indicatrix axes in 100 clinopyroxene grains from 12063,18.
   D. Crystallographic axes in same 100 grains as C.

9. Features induced by shock deformation of 12057,31.
   A. Clinopyroxene grain with shear fractures and secondary {001} twins both consistent with shock in E-W direction.
   B. Normals to faults in plagioclase (solid circles) and pyroxene (open circles) grains with shear sense indicated by small arrows. Great circles show statistical orientations of shear fractures and shear sense which are also consistent with shock wave traveling in an E-W direction.

TABLE 1

Electron Microprobe Analyses of Olivines

	12057,35				12063,18				
	1	2	3	4	5	6	7	8	9
SiO_2	36.6	35.9	34.4	36.0	36.5	37.4	36.1	26.1	31.4
MgO	34.1	30.8	27.0	28.7	32.3	33.5	28.3	0.8	0.2
FeO	29.2	32.9	37.9	35.2	31.6	29.4	36.2	69.5	70.0
MnO	0.24	0.26	0.29	0.29	0.40	0.42	0.48	0.95	0.24
CaO	0.24	0.25	0.26	0.19	0.29	0.28	0.29	0.58	0.66
Cr_2O_3	0.12	0.10	0.10	0.05	0.13	0.17	0.08	0.05	0.14
TiO_2	<0.1	<0.1	<0.1	<0.1	<0.1	<0.1	<0.1	0.14	0.02
Total	100.60	100.31	100.05	100.53	101.32	101.27	101.55	98.12	102.66

Cation Proportions Based on Four Oxygens

Z	Si	0.983	0.985	0.974	0.995	0.983	0.962	0.993	0.926	1.025
X	Mg	1.364	1.260	1.138	1.182	1.299	1.332	1.160	0.042	0.012
	Fe	0.656	0.754	0.898	0.816	0.712	0.655	0.833	2.065	1.910
	Mn	0.006	0.006	0.007	0.007	0.009	0.010	0.011	0.022	0.006
	Ca	0.007	0.007	0.008	0.006	0.009	0.008	0.009	0.022	0.023
	Cr	0.003	0.003	0.003	0.001	0.003	0.004	0.002	0.001	0.004
	Ti	---	---	---	---	---	---	---	0.004	0.001
	X	2.036	2.030	2.054	2.012	2.032	2.009	2.015	2.156	1.981
	Z	0.983	0.985	0.974	0.995	0.983	0.962	0.993	.926	1.025
	Σ	3.019	3.015	3.028	3.007	3.015	2.971	3.008	3.082	3.006
	Fo	67.52	62.56	55.89	59.16	64.59	67.04	58.20	1.99	0.62
	Fa	32.48	37.44	44.11	40.84	35.41	32.96	41.80	98.01	99.38

TABLE 2

Electron Microprobe Analyses
of
Residual Glasses in 12044,4

SiO_2	75.8	77.3
Al_2O_3	11.6	11.9
TiO_2	0.39	0.48
FeO	3.22	2.47
MgO	0.00	0.00
CaO	2.04	1.92
MnO	0.02	0.00
Na_2O	0.00	0.01
K_2O	6.97	4.81
	100.04	99.39

TABLE 3

Electron Microprobe Analyses of Twinned Pyroxene Crystal of Figure 1A (12044,4)

	1	2	3	4	5	6	7	8	9
SiO_2	47.3	47.2	49.1	48.6	49.0	50.4	49.4	49.4	52.1
Al_2O_3	1.66	1.53	1.32	1.72	1.90	0.63	2.14	2.74	1.27
TiO_2	1.15	1.08	1.03	1.15	1.46	0.73	1.77	2.13	0.86
FeO	31.2	32.1	31.4	26.5	23.0	26.5	20.5	15.8	18.3
MgO	1.79	2.57	8.30	11.0	13.1	16.7	17.2	16.5	20.7
CaO	16.0	16.0	9.7	10.1	10.8	4.76	7.9	12.1	7.3
MnO	0.39	0.39	0.40	0.32	0.30	0.29	0.32	0.30	0.29
Cr_2O_3	0.11	0.09	0.22	0.21	0.06	0.07	0.27	0.44	0.48
Total	99.60	100.96	101.47	99.60	99.62	100.08	99.50	99.41	101.30

Cation Proportions Based on Six Oxygens

Si	1.956	1.930	1.947	1.924	1.907	1.949	1.891	1.875	1.923
Al	0.044	0.070	0.053	0.076	0.087	0.029	0.097	0.123	0.055
Ti					0.016	0.021	0.012	0.002	0.022
Al	0.037	0.004	0.009	0.005					
Ti	0.036	0.033	0.031	0.034	0.027		0,039	0.059	0.007
Fe	1.078	1.098	1.041	0.876	0.748	0.855	0.655	0.501	0.565
Mg	0.110	0.157	0.491	0.649	0.760	0.963	0.979	0.931	1.140
Ca	0.707	0.703	0.410	0.429	0.450	0.197	0.324	0.493	0.288
Mn	0.015	0.013	0.012	0.010	0.009	0.008	0.008	0.010	0.009
Cr	0.004	0.003	0.007	0.007	0.007	0.002	0.008	0.013	0.014
Z	2.000	2.000	2.000	2.000	2.000	1.999	2.000	2.000	2.000
X	1.987	2.011	2.001	2.010	2.001	2.025	2.013	2.007	2.023
Σ	3.987	4.011	4.001	4.010	4.001	4.024	4.013	4.007	4.023
Fs	56.89	56.08	53.60	44.83	38.20	42.93	33.45	26.03	28.35
% En	5.80	8.02	25.28	33.21	38.82	47.79	50.00	48.36	57.20
Wo	37.31	35.90	21.12	21.96	22.98	9.28	16.55	25.61	14.45

TABLE 4

Electron Microprobe Analyses of Pigeonite-cored Clinopyroxene Crystal of Figure 1B (12044,4)

	1	2	3	4	5	6	7	8	9	10	11	12	13
SiO_2	50.3	51.0	52.1	53.7	51.9	50.7	50.2	52.8	52.1	53.4	51.7	51.3	50.5
Al_2O_3	3.73	2.68	2.02	0.91	1.99	3.06	3.58	0.98	1.20	1.59	1.63	1.67	1.36
TiO_2	2.23	1.81	1.67	0.97	1.07	1.78	1.93	0.71	0.67	0.92	1.15	0.86	1.21
FeO	13.7	15.6	18.5	18.9	18.1	13.8	13.4	20.1	19.0	18.4	16.9	21.9	27.1
MgO	15.3	16.8	17.9	21.8	20.6	16.6	15.6	22.5	21.2	20.3	19.6	17.2	11.5
CaO	15.3	11.4	6.8	4.04	6.5	13.9	13.4	3.72	5.8	6.6	9.3	8.2	7.3
MnO	0.25	0.30	0.31	0.32	0.31	0.28	0.24	0.31	0.33	0.34	0.36	0.34	0.33
Cr_2O_3	0.78	1.04	0.68	0.67	0.71	0.78	1.00	0.46	0.43	0.33	0.38	0.19	0.11
Total	101.59	100.63	99.98	101.31	101.18	100.90	99.35	101.58	100.73	101.88	101.02	101.66	99.41

Cation Proportions Based on Six Oxygens

Z	Si	1.859	1.898	1.945	1.962	1.911	1.881	1.885	1.941	1.934	1.954	1.917	1.923	1.979
	Al	0.141	0.102	0.055	0.038	0.087	0.119	0.115	0.042	0.053	0.046	0.071	0.074	0.021
	Ti					0.002			0.017	0.013		0.012	0.003	
WXY	Al	0.022	0.015	0.034	0.001		0.015	0.043			0.023			0.041
	Ti	0.062	0.050	0.047	0.027	0.028	0.050	0.054	0.003	0.006	0.026	0.020	0.021	0.036
	Fe	0.424	0.486	0.576	0.578	0.559	0.478	0.421	0.617	0.590	0.561	0.525	0.688	0.890
	Mg	0.841	0.929	0.997	1.188	1.131	0.918	0.874	1.231	1.176	1.106	1.084	0.964	0.673
	Ca	0.607	0.455	0.272	0.159	0.258	0.552	0.538	0.147	0.229	0.258	0.371	0.329	0.309
	Mn	0.008	0.009	0.009	0.010	0.010	0.009	0.008	0.009	0.010	0.010	0.011	0.010	0.010
	Cr	0.018	0.031	0.020	0.019	0.021	0.023	0.030	0.014	0.012	0.010	0.011	0.006	0.004
	Z	2.000	2.000	2.000	2.000	2.000	2.000	2.000	2.000	2.000	2.000	2.000	2.000	2.000
	X	1.982	1.975	1.955	1.982	2.007	2.045	1.968	2.021	2.023	1.994	2.022	2.008	1.963
	Σ	3.982	3.975	3.955	3.982	4.007	4.045	3.968	4.021	4.023	3.994	4.022	4.008	3.963
Mol%	Fs	22.65	25.99	31.22	30.03	28.70	24.54	26.08	30.93	29.57	29.14	26.52	34.73	47.54
	En	44.93	49.68	54.04	61.71	58.06	47.13	47.68	61.70	58.95	57.45	54.75	48.66	35.95
	Wo	32.42	24.33	14.74	8.26	13.24	28.33	29.34	7.37	11.48	13.41	18.73	16.61	16.51

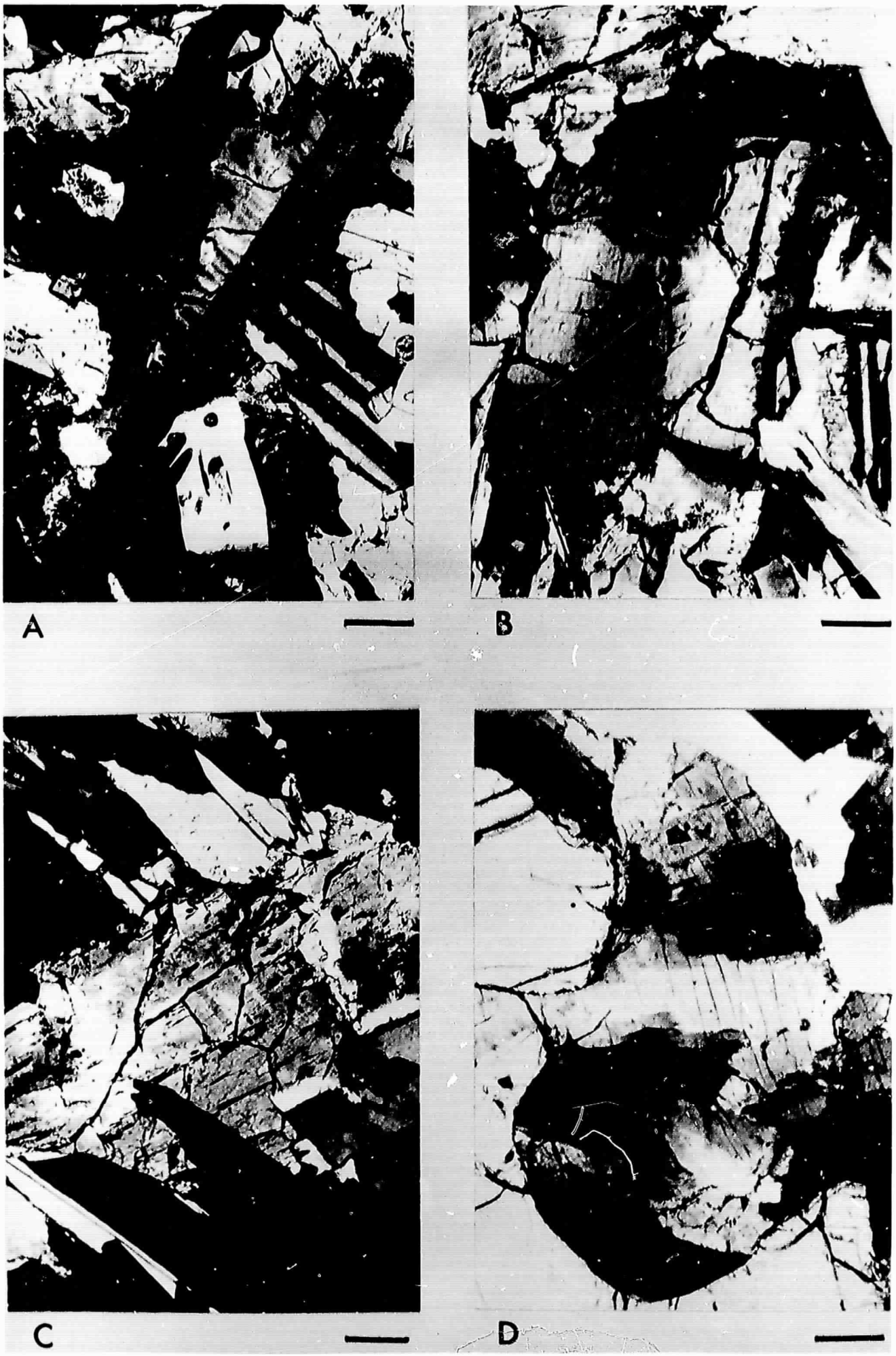
A
B
C
D

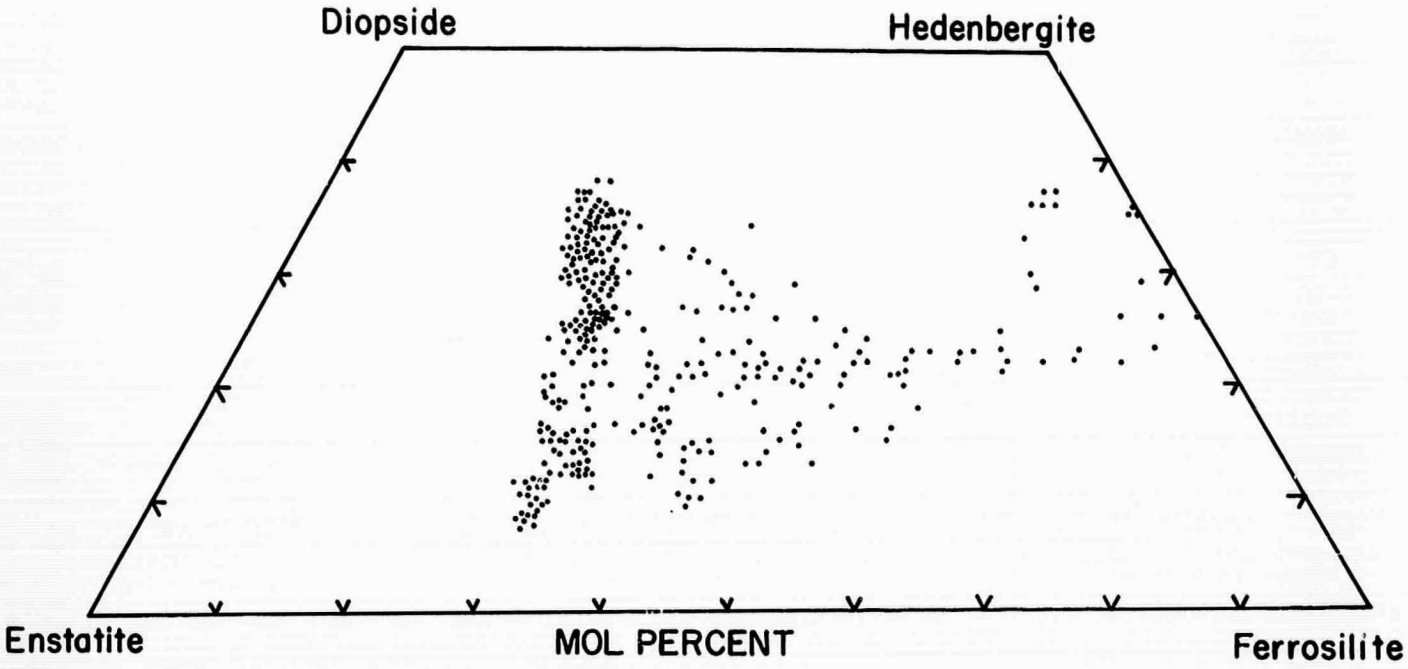
Diopside
Hedenbergite
Enstatite
MOL PERCENT
Ferrosilite

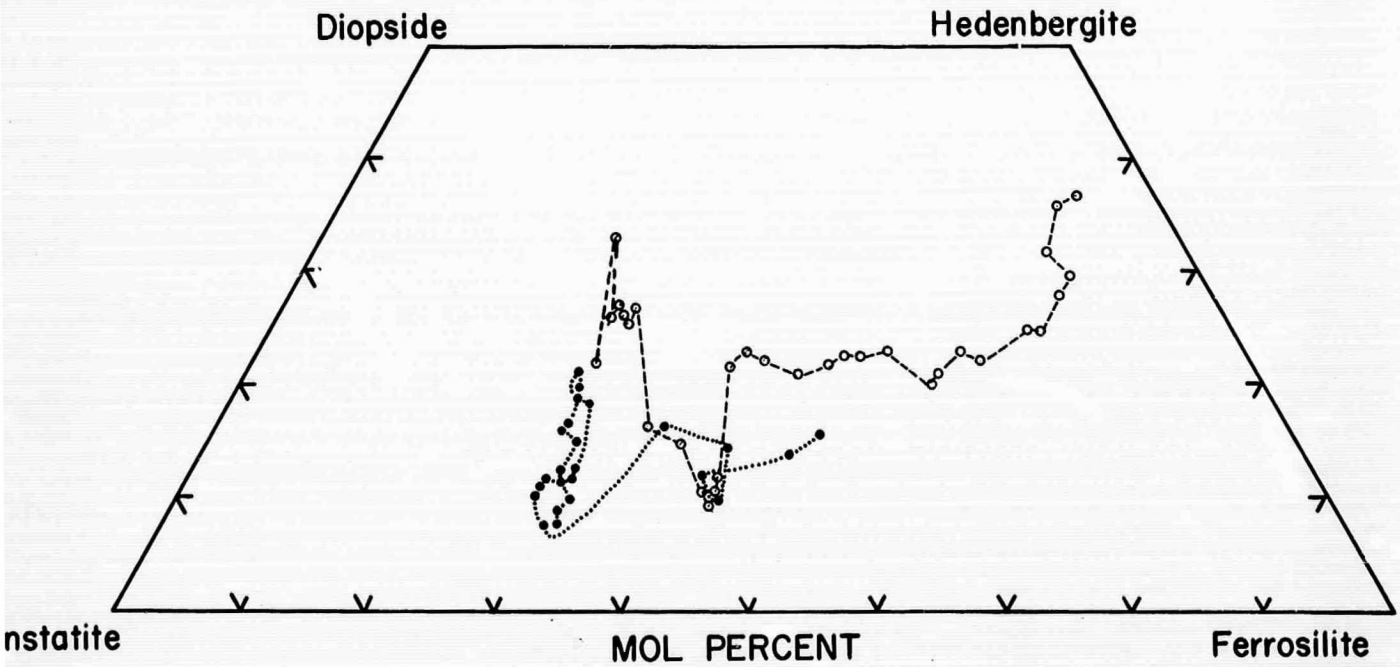
Diopside
Hedenbergite
nstatite
MOL PERCENT
Ferrosilite

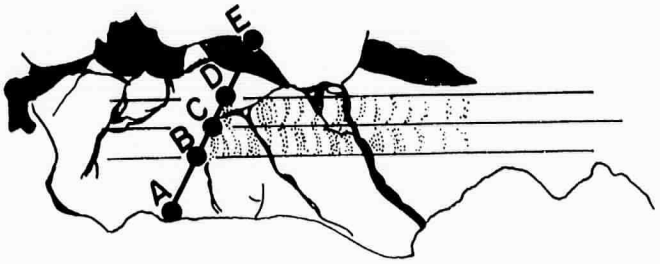

Si

Mn

Cr

Mg

Ti

Ca

Fe

Al

A B C D E

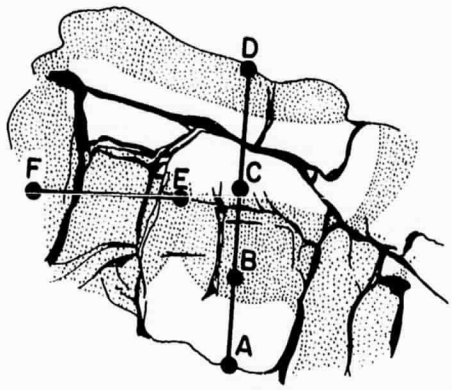

Si

Cr

Mn

Fe

Mg

Ti

Al

Ca

A B C D E F

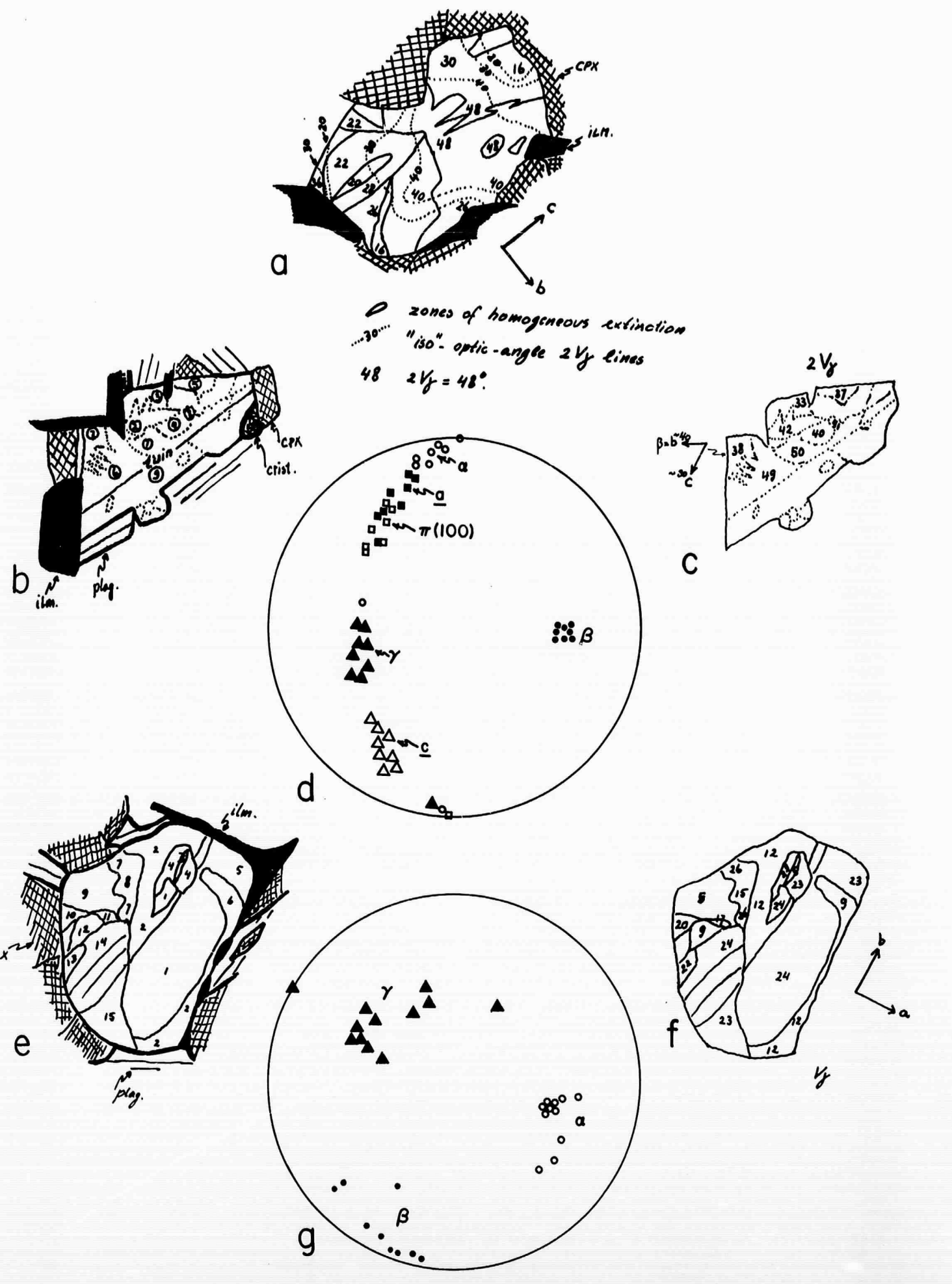
a
CPX
ilm.
c
b
zones of homogeneous extinction
"isogyre" - optic-angle $2V_\gamma$ lines
48 $2V_\gamma = 48°$
b
ilm.
plag.
quin
CPX
crist.
c
$2V_\gamma$
$\beta = b$
~30°
c
d
α
a
π(100)
β
γ
c
e
ilm.
plag.
x
f
b
a
V_γ
g
γ
α
β


A
B
C
D

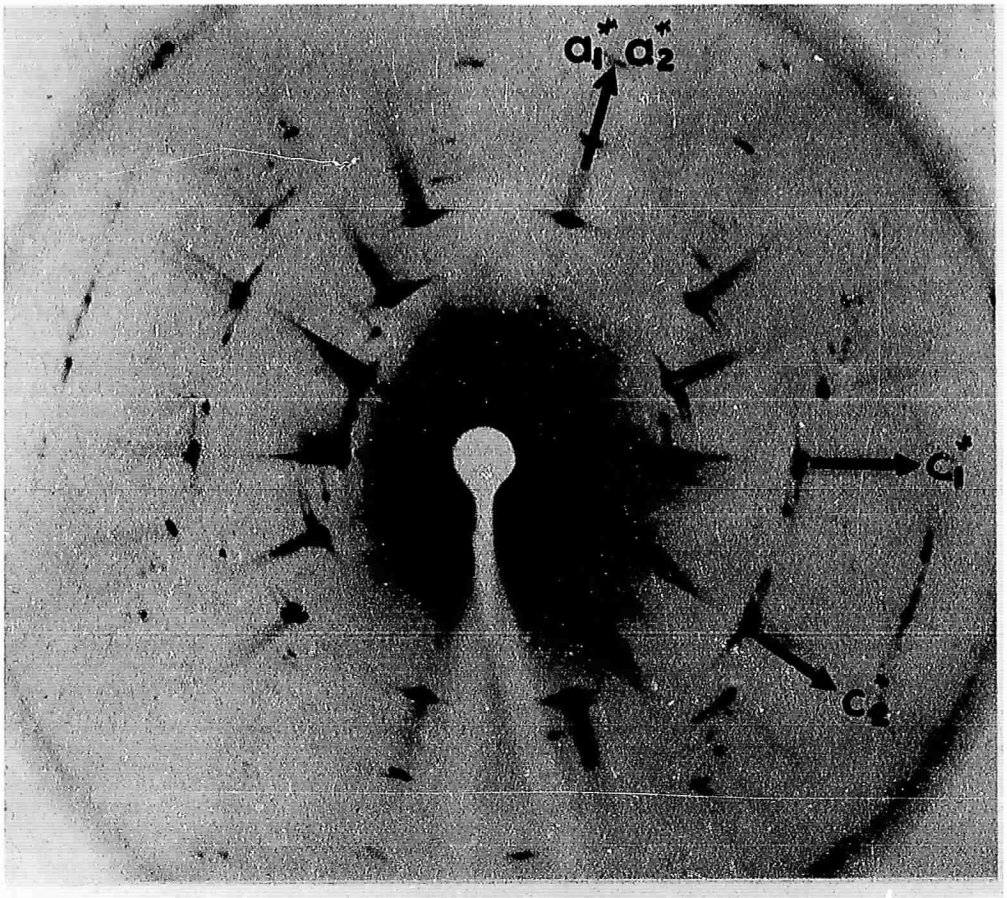

A

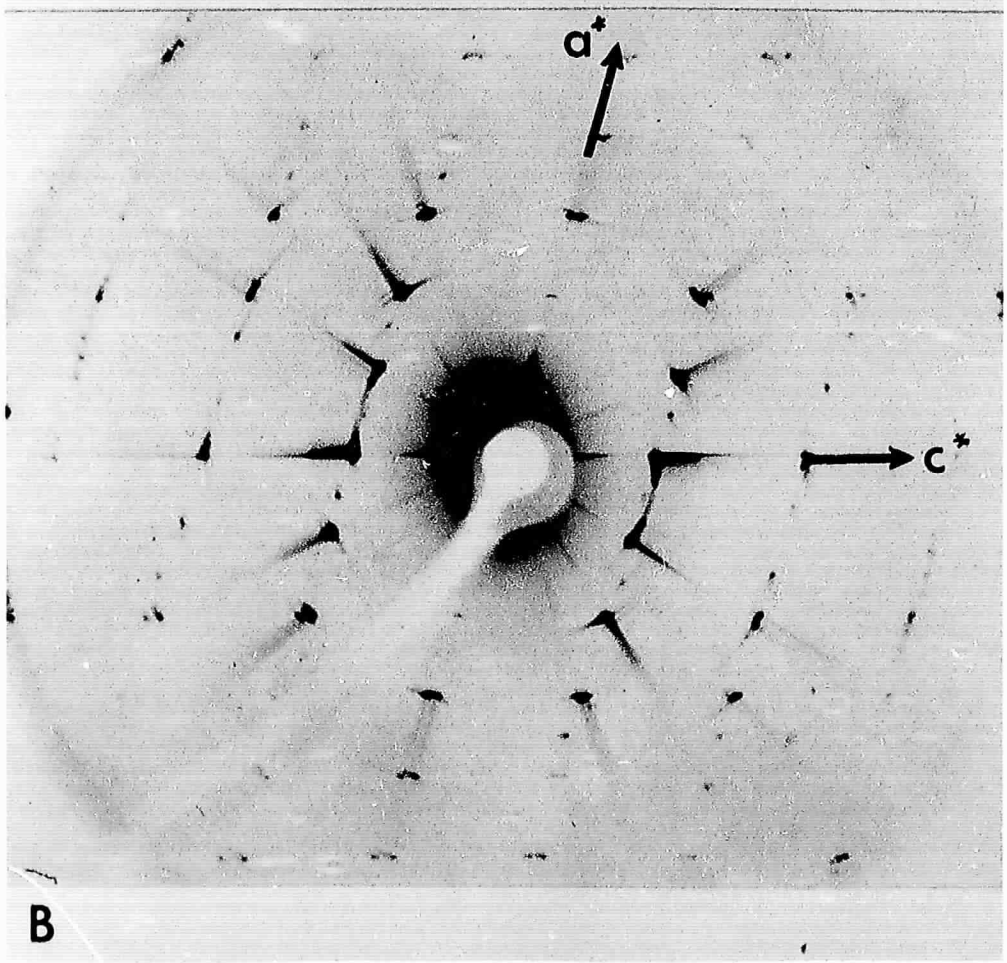

B

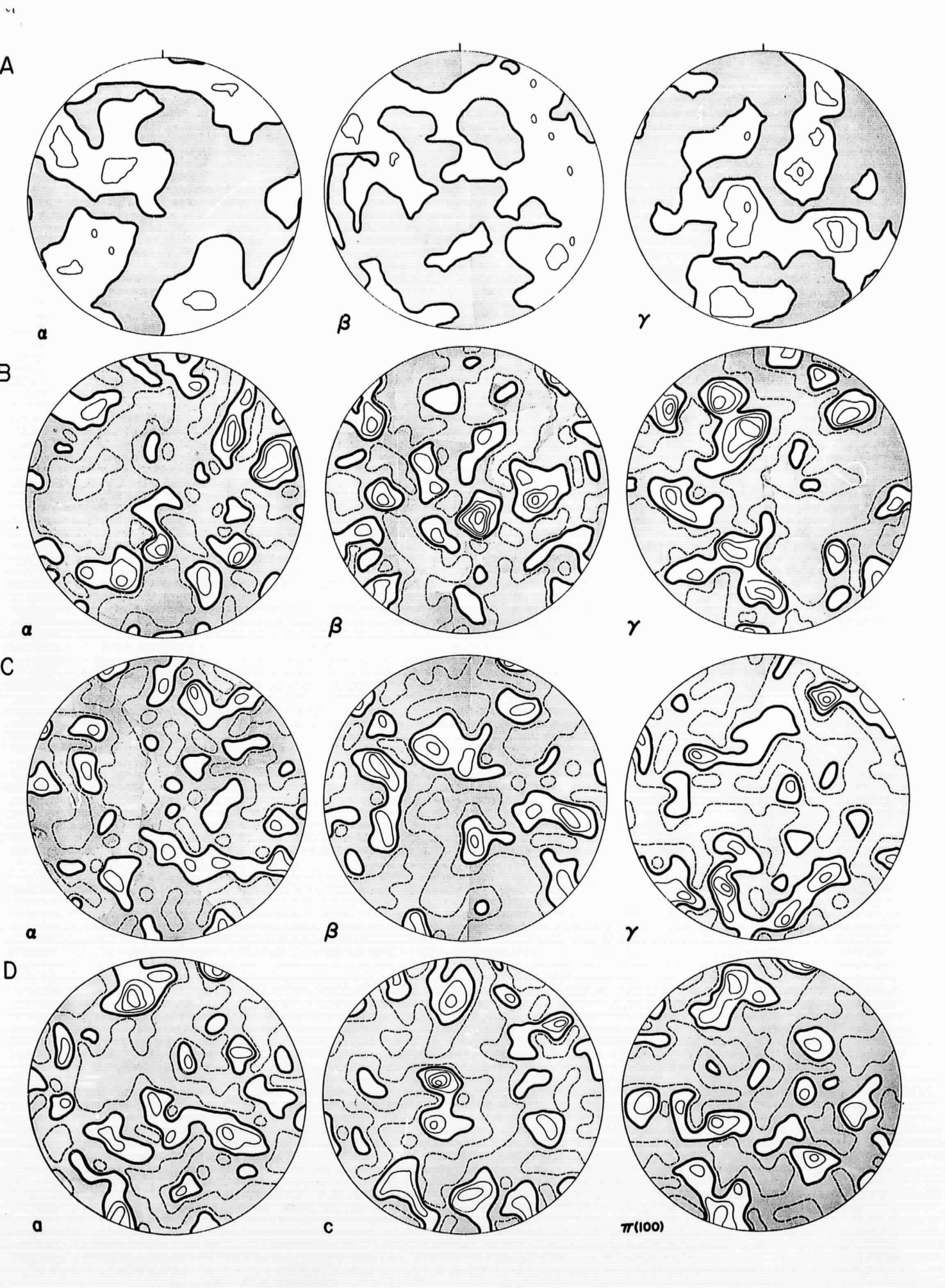
A
α
β
γ
B
α
β
γ
C
α
β
γ
D
a
c
π(100)

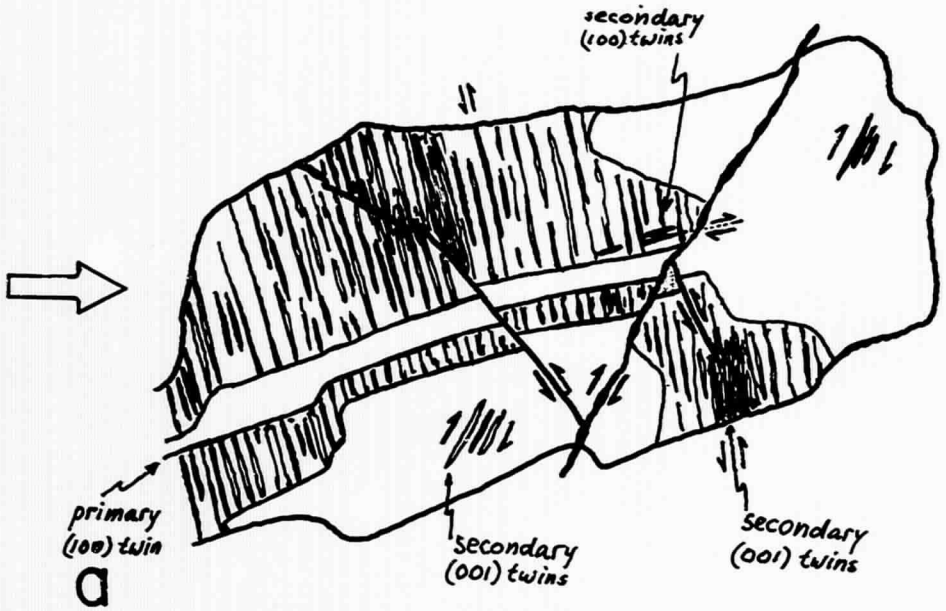
secondary
(100) twins
primary
(100) twin
secondary
(001) twins
secondary
(001) twins
a

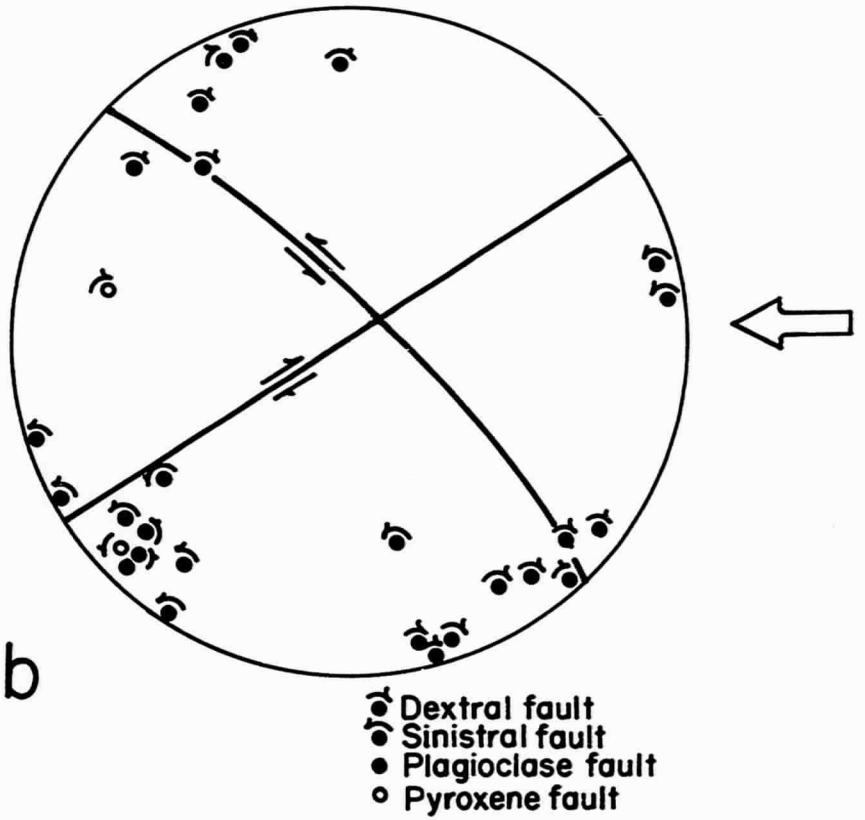
b
Dextral fault
Sinistral fault
Plagioclase fault
Pyroxene fault